JOURNAL OF VIROLOGY, Mar. 2009, p. 2298–2309 Vol. 83, No. 5
0022-538X/09/$08.00+0 doi:10.1128/JVI.01245-08

Severe Acute Respiratory Syndrome Coronavirus Triggers Apoptosis via Protein Kinase R but Is Resistant to Its Antiviral Activity▽

Verena Krähling,[1] David A. Stein,[2] Martin Spiegel,[3,4] Friedemann Weber,[4] and Elke Mühlberger[1,5,6]*

Department of Virology, Philipps University Marburg, Hans-Meerwein-Strasse 2, 35043 Marburg, Germany[1]; Department of Microbiology, Oregon State University, Corvallis, Oregon[2]; Institute of Virology, Georg August University Göttingen, Kreuzbergring 57, 37075 Göttingen, Germany[3]; Department of Virology, Institute for Medical Microbiology and Hygiene, Hermann-Herder-Strasse 11, 79104 Freiburg, Germany[4]; and National Emerging Infectious Diseases Laboratories Institute[5] and Department of Microbiology, Boston University School of Medicine,[6] 72 East Concord Street, Boston, Massachusetts

Received 16 June 2008/Accepted 15 December 2008

In this study, infection of 293/ACE2 cells with severe acute respiratory syndrome coronavirus (SARS-CoV) activated several apoptosis-associated events, namely, cleavage of caspase-3, caspase-8, and poly(ADP-ribose) polymerase 1 (PARP), and chromatin condensation and the phosphorylation and hence inactivation of the eukaryotic translation initiation factor 2α (eIF2α). In addition, two of the three cellular eIF2α kinases known to be virus induced, protein kinase R (PKR) and PKR-like endoplasmic reticulum kinase (PERK), were activated by SARS-CoV. The third kinase, general control nonderepressible-2 kinase (GCN2), was not activated, but late in infection the level of GCN2 protein was significantly reduced. Reverse transcription-PCR analyses revealed that the reduction of GCN2 protein was not due to decreased transcription or stability of GCN2 mRNA. The specific reduction of PKR protein expression by antisense peptide-conjugated phosphorodiamidate morpholino oligomers strongly reduced cleavage of PARP in infected cells. Surprisingly, the knockdown of PKR neither enhanced SARS-CoV replication nor abrogated SARS-CoV-induced eIF2α phosphorylation. Pretreatment of cells with beta interferon prior to SARS-CoV infection led to a significant decrease in PERK activation, eIF2α phosphorylation, and SARS-CoV replication. The various effects of beta interferon treatment were found to function independently on the expression of PKR. Our results show that SARS-CoV infection activates PKR and PERK, leading to sustained eIF2α phosphorylation. However, virus replication was not impaired by these events, suggesting that SARS-CoV possesses a mechanism to overcome the inhibitory effects of phosphorylated eIF2α on viral mRNA translation. Furthermore, our data suggest that viral activation of PKR can lead to apoptosis via a pathway that is independent of eIF2α phosphorylation.

In March 2003, a novel coronavirus (CoV) was identified as the causative agent of severe acute respiratory syndrome (SARS) in humans (37, 53). CoVs, as members of the order *Nidovirales*, are enveloped viruses with a single-stranded positive-sense RNA genome of approximately 30,000 nucleotides (nt) in length. CoVs infect a broad range of vertebrates and can cause a variety of disorders, including gastroenteritis and respiratory tract diseases (38). The human CoVs identified to date, hCoV-229E, hCoV-OC43, hCoV-NL63, and hCoV-HKU-1, cause primarily mild respiratory diseases with common-cold-like symptoms. In contrast, SARS-CoV is highly pathogenic in humans, causing severe damage to the upper and lower respiratory systems, lymphopenia, and thrombocytopenia (12, 52, 81) with a mortality rate of about 10% (79).

Autopsy studies have revealed that the cells in various SARS-CoV-infected tissues, such as lung, spleen, and thyroid, exhibited hallmark indications of apoptosis (77, 87). These observations suggest that modulation of apoptosis during infection could be important for viral replication and pathogenesis. Indeed, results from overexpression studies have suggested that many different SARS-CoV proteins have the ability to induce apoptosis (10, 35, 60, 70, 72, 83). However, little is known about the mechanisms leading to apoptosis in SARS-CoV-infected cells.

The initial response to viral infection in mammals includes the production of cytokines such as the type I interferons (IFN-α and -β). Once bound to their receptors at the cell surface, IFNs activate the Janus kinase signaling cascade, which leads to the expression of a spectrum of cellular genes (24, 25). Among those is the protein kinase regulated by RNA, protein kinase R (PKR), a key effector of IFN-mediated antiviral action. PKR is a serine/threonine kinase characterized by two distinct kinase activities. In addition to the autophosphorylation activity of PKR (which mediates activation), the best-characterized substrate of PKR is the α subunit of the eukaryotic translation initiation factor 2 (eIF2α) (57). Autophosphorylation of PKR is induced upon its binding of double-stranded RNA (dsRNA) or 5′-triphosphate RNA (48), which in turn results in the phosphorylation of the serine at position 51 of eIF2α (15, 73). Phosphorylation of eIF2α renders eIF2 to an inactive form and causes inhibition of host cell translation initiation, frequently leading to apoptosis (61). The link between eIF2α phosphorylation and induction of apoptosis was first established by showing that PKR-mediated apoptosis is reduced in the presence of eIF2α that has been mutagenized to contain a nonphosphorylatable Ala at the position of Ser51 (22, 63).

In addition to PKR, two other virus-activated kinases are known to phosphorylate eIF2α: (i) the PKR-like endoplasmic

* Corresponding author. Mailing address: Department of Microbiology, Boston University School of Medicine, 72 East Concord Street, Boston, MA 02118. Phone: (617) 638-0336. Fax: (617) 638-4286. E-mail: muehlber@bu.edu.

▽ Published ahead of print on 24 December 2008.

TABLE 1. PPMO names, sequences, and target locations in human PKR mRNA

PPMO compound	PPMO target location (nt)	PPMO sequence (5′→3′)
"Scramble"	NA[a]	AGT CTC GAC TTG CTA CCT CA
"AUG"	426–447 (initiator-AUG of mRNA)	ATC ACC AGC CAT TTC TTC TTC C
5′ED	17–38 (5′ untranslated region)	AGT CAC AAA GTA TGA GCA AAC T
ex-7	956–977 (5′ end of exon 7, near splice site in pre-mRNA)	GAA CCA GAG GAC AGG TAG TCA G
ex-8	1028–1052 (5′ end of exon 8, near splice site in pre-mRNA)	CCT TCA GAT GAT GAT TCA GAA GCG

[a] NA, not applicable.

reticulum (ER) kinase (PERK), which can be activated by unfolded proteins in the ER (27, 78), and (ii) the general control nonderepressible-2 kinase (GCN2), which is activated by UV irradiation, amino acid deprivation, and certain viral RNA sequences (5). To date, there is no evidence that a fourth cellular eIF2α kinase, heme-regulated inhibitor kinase, is activated due to virus infections. Heme-regulated inhibitor kinase has been shown to be activated by heme deficiency or under conditions of heat shock or oxidative stress (13, 14).

dsRNA, the activator of PKR, is produced in large amounts during viral replication in SARS-CoV-infected cells (76). The purpose of this study was to address the biochemistry of PKR activation in SARS-CoV-infected cells and how such activation affects the efficiency of virus replication and contributes to the induction of apoptosis. We found that both PKR and PERK are activated in SARS-CoV-infected cells, leading to sustained phosphorylation of eIF2α. Moreover, downregulation of PKR led to a significant reduction of poly(ADP-ribose) polymerase 1 (PARP) cleavage in infected cells but did not affect virus growth.

(V. Krähling performed this work in partial fulfillment of the requirements for a Ph.D. degree from the Philipps University of Marburg, Marburg, Germany.)

MATERIALS AND METHODS

Cells and viruses. 293 low-passage cells (PD-02-01; Microbix Bisosystems Inc.) and 293/ACE2 cells (33) (kindly provided by Shinji Makino, UTMB, Galveston, Texas) were cultured in Dulbecco's modified Eagle medium (DMEM) supplemented with 10% fetal calf serum (FCS), penicillin (50 units/ml), and streptomycin (50 μg/ml). Selection of 293/ACE2 cells constitutively expressing human angiotensin-converting enzyme 2 (ACE2) was performed by addition of blasticidin at a concentration of 12 μg per ml medium. The FFM-1 isolate of SARS-CoV (GenBank accession number AY310120) and vesicular stomatitis virus (VSV) strain Indiana were propagated in Vero E6 cells. Virus titers of SARS-CoV and VSV were determined by 50% tissue culture infectious dose ($TCID_{50}$) assays. Sendai virus (SeV) strain Cantell (kindly provided by C. F. Basler, Mount Sinai School of Medicine, New York) was propagated in 11-day-old embryonated chicken eggs. SeV hemagglutinating units/ml were determined by a standard hemagglutination test. All work with SARS-CoV was performed in the biosafety level 4 facility of the University of Marburg.

$TCID_{50}$ assay. Vero E6 cells were cultured in 96-well plates to 50% confluence and infected with 10-fold serial dilutions of supernatants from cells that were infected and/or treated with peptide-conjugated phosphorodiamidate morpholino oligomers (PPMO) and/or IFN-β. At 3 to 8 days post infection (p.i.), when the cytopathic effect had stabilized to a constant rate, cells were analyzed by light microscopy. The $TCID_{50}$/ml was calculated using the Spearman-Kärber method (28).

Immunofluorescence analysis. At the indicated times p.i., infected cells were fixed with 4% paraformaldehyde in DMEM for at least 12 h. Thereafter, cells were permeabilized with 0.1% Triton X-100 for 10 min, treated with 0.1 M glycine for 10 min, and subsequently incubated in blocking reagent (2% bovine serum albumin, 0.2% Tween 20, 3% glycerin, and 0.05% NaN_3 in phosphate-buffered saline deficient in Mg^{2+} and Ca^{2+}) for 15 min. Immunofluorescence analyses were performed as described elsewhere (7) using a rabbit antiserum directed against the nucleoprotein of SARS-CoV (dilution, 1:1,000; kindly provided by L. Martínez-Sobrido and A. Garcia-Sastre, Mount Sinai School of Medicine, New York) or an antibody directed against SeV (dilution, 1:500; kindly provided by W. J. Neubert, Max Planck Institute, Martinsried, Germany). Infected cells were additionally analyzed for the presence of dsRNA by using J2 monoclonal antibody (English & Scientific Consulting; dilution, 1:100). Bound antibodies were detected with either rhodamine-labeled goat anti-rabbit immunoglobulin G or rhodamine-labeled goat anti-mouse immunoglobulin G (dilution, 1:100; Dianova).

Western blot analysis. Whole-cell extracts were prepared by incubating cells in cell lysis buffer (10 mM Tris [pH 7.4], 100 mM NaCl, 1 mM EDTA, 1 mM EGTA, 1 mM NaF, 20 mM $Na_4P_2O_7$, 2 mM Na_3VO_4, 1% Triton, 10% glycerol, 0.1% sodium dodecyl sulfate [SDS], 0.5% deoxycholate) for 20 min on ice. Protease inhibitor mixture (1× Complete tablets; Roche) and the serine/threonine phosphatase inhibitor Calyculin A (Cell Signaling; 0.1 μM) were added to cell lysis buffer prior to incubation. To analyze cleavage of procaspase-3 and -8 cells were lysed in 50 μl of 1× CHAPS {3-[(3-cholamidopropyl)-dimethylammonio]-1-propanesulfonate} buffer (Cell Signaling) containing 1 mM protease inhibitor mix (1× Complete tablets; Roche) and 5 mM dithiothreitol, followed by three freeze-and-thaw cycles. The extracts from both lysing methods were then centrifuged and supernatants transferred to fresh tubes containing 2× SDS sample buffer (25% glycerol, 2.5% SDS, 125 mM Tris [pH 6.8], 125 mM dithiothreitol, 0.25% bromophenol blue). Proteins were separated on 8 to 15% SDS-polyacrylamide gels and transferred onto polyvinylidene difluoride membranes. Immunostaining was performed with an appropriate dilution of primary antibody in phosphate-buffered saline or Tris-buffered saline containing either 5% (wt/vol) skim milk or 5% (wt/vol) bovine serum albumin according to the manufacturer's instructions. Rabbit (unless otherwise stated) polyclonal antibodies were used to detect human PARP (Cell Signaling; 1:1,000), phosphorylated eIF2α (Ser51) (Biosource; 1:30,000), PKR (mouse, BD Bioscience; 1:30,000), PERK (Santa Cruz Biotechnology; 1:1,000), phospho-PERK (Thr980) (BioLegend; 1:1,000), GCN2 (Cell Signaling; 1:5,000), phospho-GCN2 (Cell Signaling; 1:1,000), and caspase-3 (monoclonal, Cell Signaling; 1:1,000); mouse (unless otherwise stated) monoclonal antibodies were used to detect eIF2α (Biosource; 1:1,000), phospho-PKR (pT446) (rabbit, Epitomics; 1:1,000), caspase-8 (Cell Signaling; 1:1,000), and β-actin (ab8226, Abcam; 1:40,000); and a rabbit antiserum was used to detect the nucleoprotein of SARS-CoV (dilution, 1:10,000). Western blot detection was done with horseradish peroxidase-conjugated anti-rabbit immunoglobulin G or anti-mouse immunoglobulin G secondary antibody using an enhanced chemiluminescence detection reagent kit (Pierce) according to the manufacturer's protocol. Immunoreactive bands were visualized using an Optimax 2010 imaging system (Protec processor technology) with high-performance chemiluminescence films (GE Healthcare).

Design and synthesis of PPMO. Phosphorodiamidate morpholino oligomers (PMO) are single-stranded antisense agents that possess DNA purine and pyrimidine bases attached to a backbone consisting of morpholine rings joined by phosphorodiamidate linkages and were synthesized as previously described (68). To enhance uptake into cells, all PMO were conjugated at the 5′end through a noncleavable linker to the cell-penetrating peptide $(RXR)_4XB$ (R is arginine, X is 6-aminohexanoic acid, and B is beta-alanine) to produce PPMO by methods previously described (2). Four different PKR-specific PPMO were designed to target human PKR mRNA (GenBank accession number BC057805). The sequences and exact target locations of the PPMO are defined in Table 1. PPMO 5′ED and "AUG" target sequences near the 5′ terminus and the AUG transla-

tion initiation site, respectively, of the PKR mRNA. PPMO ex-7 and ex-8 were designed against exonic sequences near the intron/exon splice junctions for exons 7 and 8, respectively, of the pre-mRNA (derived from the sequence under GenBank accession number BC057805), in an effort to disrupt mRNA processing. A PPMO of random sequence (scramble) was synthesized to serve as a control for off-target effects.

RT-PCR. 293 or 293/ACE2 cells were seeded into six-well culture plates at a concentration of 4×10^4 cells per well and allowed to adhere overnight. For detection of PKR mRNA after PPMO treatment, cells were treated with 20 μM PPMO in 1 ml DMEM containing penicillin (50 units/ml), streptomycin (50 μg/ml), and 2% FCS (DMEM+) or with DMEM+ alone; 48 h later, total cellular RNA was isolated using the RNeasy minikit (Qiagen). For detection of PKR, GCN2, and glyceraldehyde 3-phosphate dehydrogenase (GAPDH) mRNAs in SARS-CoV-infected cells, cells were infected with SARS-CoV (multiplicity of infection [MOI] of 0.01) or mock infected, and total cellular RNA was isolated at 8, 24, and 48 h p.i. One-eighth of the volume of eluted RNA (5 μl) was used for reverse transcription-PCR (RT-PCR) using the OneStep RT-PCR kit (Qiagen) and PKR-specific primers (forward, 5′-GGTTTCTTCATGGAGGAA CTTAATAC; reverse, 5′-TAGAGGTCCACTTCCTTTCCA) designed to amplify nt 457 to 1850 of human PKR mRNA, GCN2-specific primers (forward, 5′-GAAGGCACCGTCAAGATTACG; reverse, 5′-GACTCTGTACCACACC TTGATG), or GAPDH-specific primers (forward, 5′-TGAAGGTCGGAGTCA ACGGA; reverse, 5′-CATGTGGGCCATGAGGTCCA). Ten percent of each RT-PCR mixture was resolved on a 1.5% agarose gel and stained with ethidium bromide. RT-PCR products produced from RNA isolated from PPMO-treated cells were sequenced. To analyze cellular RNA levels, 1 μl of extracted RNA was resolved on a 1.5% agarose gel and stained with ethidium bromide.

ISG-54 reporter gene assay. Transfection of 293 cells was performed using Lipofectamine 2000 (Invitrogen) according to the manufacturer's instructions. A total of 4×10^4 cells were transfected with 0.8 μg of the IFN-stimulated response element-driven firefly luciferase reporter plasmid pHISG-54-Luc (a kind gift of D. Levy, New York University School of Medicine, New York) along with 0.2 μg of the constitutive *Renilla* luciferase expression plasmid pRL-SV40 (Promega). At 24 h posttransfection, cells were either infected with SeV or treated with 20 μM PPMO; 48 h later, cells were harvested and lysed in passive lysis buffer (Promega) for luciferase assays. Luciferase assays were performed by using the Promega dual luciferase assay system according to the manufacturer's instructions. Relative *Renilla* luciferase production was used to normalize for transfection efficiency.

Infection of cells, PPMO treatment, and IFN-β treatment. Unless otherwise stated, 4×10^4 293/ACE2 cells were seeded in six-well culture plates and treated the next day with a final concentration of 20 μM PPMO in DMEM+, or DMEM+ alone, for 72 h. Subsequently, PPMO-containing medium was removed and the cells then either infected with SARS-CoV or further treated with 10,000 international units (IU) of IFN-β for 24 h prior to infection with SARS-CoV at an MOI of 0.01 as indicated. After an infection period of 1 h, the supernatant was removed and replaced by DMEM+ or by DMEM+ containing 20 μM of appropriate PPMO, and the cells were then further incubated for 24 to 48 h.

RESULTS

SARS-CoV infection induces apoptosis in 293/ACE2 cells. Cell culture demonstrations that SARS-CoV induces apoptosis have typically been conducted with Vero E6 cells, an African green monkey kidney cell line (8, 47, 55, 70, 80). However, Vero cells are less than optimal for investigating human host-virus interactions, in part because many of their cellular proteins are not recognized by available antibodies. We therefore sought to determine if human 293/ACE2 cells stably expressing the SARS-CoV receptor (33) undergo apoptosis after infection with SARS-CoV, as Vero cells do. 293/ACE2 cells were inoculated with SeV, VSV, or SARS-CoV, and cell lysates were analyzed for cleavage of PARP, a reliable indicator for late-stage apoptosis and a generally accepted hallmark of apoptosis. PARP, a 113-kDa nuclear zinc finger protein, is a DNA nick sensor that functions in the DNA repair processes. During apoptosis, PARP is cleaved by caspases into two inactive fragments (89 kDa and 24 kDa) (31). VSV and SeV both are known to be potent inducers of apoptosis (6, 41). In 293/ACE2 cells infected with either virus, PARP cleavage was detectable at 24 h p.i. and robust at 48 h p.i., indicating that these cells undergo apoptosis in response to infection (Fig. 1A). In 293/ACE2 cells infected with SARS-CoV, cleavage of PARP was not detectable at 24 h, although almost all cells were infected (Fig. 1A and E). However, PARP cleavage was clearly evident at 48 h p.i. and was prominent at 72 h p.i. In noninfected cells PARP cleavage was nondetectable at 48 h but prominent at 72 h, suggesting that the high density of cells that had accumulated at this late time point caused induction of apoptosis (Fig. 1A). To confirm the finding that SARS-CoV induces apoptosis in 293/ACE2 cells, cleavage of effector caspase-3 and initiator caspase-8 was analyzed. As shown in Fig. 1B, caspase-3 cleavage was observed at 48 h and 72 h p.i., thus temporally coinciding with PARP cleavage. Cleavage of caspase-3 was also observed in noninfected cells at 72 h p.i., but the proportion of uncleaved to cleaved caspase-3 was much higher in noninfected than in infected cells (Fig. 1B). The total amount of (uncleaved) procaspase-8 was significantly lower in infected cells than in noninfected cells at all three time points tested. At 24 or 48 h p.i., the cleavage product of caspase-8 could not be detected in either infected or noninfected cells. However, at 72 h p.i., a weak band corresponding to cleaved caspase-8 was detected in the infected but not in the noninfected cells (Fig. 1B), providing a further indication of virus-induced apoptosis. Finally, chromatin condensation, considered an indicator for late-stage apoptosis, was observed in SARS-CoV-infected cells at 48 h and 72 h p.i. (Fig. 1C). SARS-CoV N protein was detectable as early as 8 h p.i., reached a robust level by 24 h p.i., and remained at a high level through 72 h p.i. (Fig. 1D). It has previously been shown that SARS-CoV is a fast-replicating virus. Stertz et al. (65) observed budding of SARS-CoV at intracellular membranes at 3 h p.i., and Ng et al. (51) observed virus particle release from infected cells at 5 h p.i. The results shown in Fig. 1A to D suggest that the induction of apoptosis in SARS-CoV-infected 293/ACE2 cells occurred during the later stages of infection.

eIF2α and PKR are phosphorylated in SARS-CoV-infected cells. Apoptosis is a complex cellular process which can be induced in many ways. Since it is known that virus-induced phosphorylation of eIF2α eventually results in the induction of apoptosis (34, 86), we analyzed whether eIF2α becomes phosphorylated in SARS-CoV-infected cells. 293/ACE2 cells were infected with SARS-CoV, harvested at various times p.i., and subjected to Western blot analysis. eIF2α phosphorylation was observed at 8 and 24 h p.i. in SARS-CoV-infected cells (Fig. 2A, upper panel).

Currently, three kinases (PKR, PERK, and GCN2) are known to phosphorylate eIF2α in response to viral stimuli. Since PKR is activated by dsRNA and since dsRNA reportedly becomes abundant in SARS-CoV-infected cells (76), we initially focused on PKR as the kinase most likely to be responsible for eIF2α phosphorylation in SARS-CoV-infected 293/ACE2 cells. We observed that dsRNA was indeed present in large amounts in SARS-CoV-infected 293/ACE2 cells (Fig. 2B) and that PKR was phosphorylated at 8 and 24 h p.i., demonstrating that the processes of PKR activation and eIF2α phosphorylation temporally coincide in SARS-CoV-infected cells (Fig. 2A). The observed eIF2α phosphorylation in non-

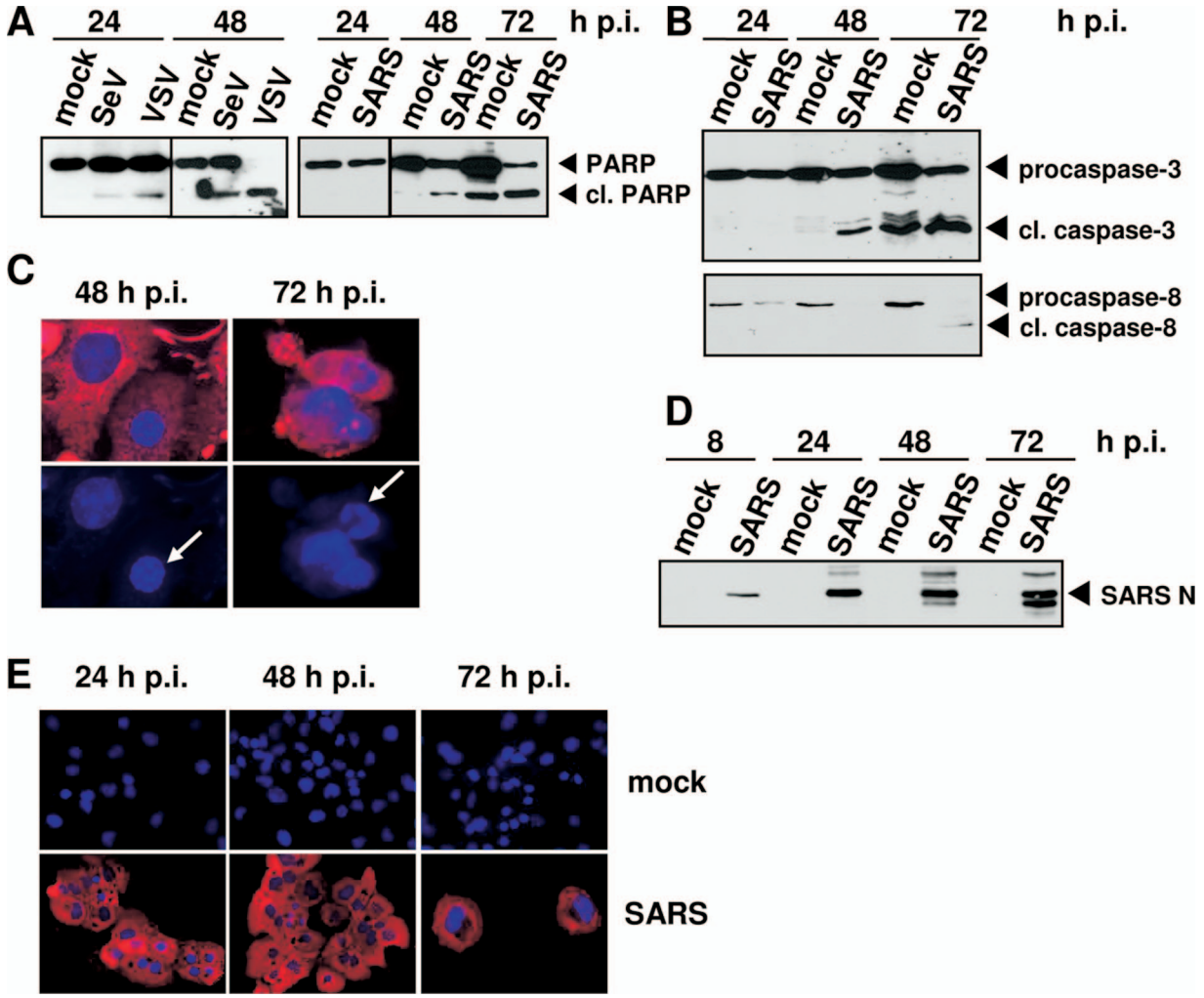

FIG. 1. Induction of apoptosis in SARS-CoV-infected 293/ACE2 cells. (A) 293/ACE2 cells were infected with VSV (MOI, 0.01), SeV (20 hemagglutinating units), or SARS-CoV (MOI, 0.01). Protein extracts from samples collected at different time points p.i. were subject to Western blot analysis using anti-PARP antibody. (B) 293/ACE2 cells were infected with SARS-CoV as described for panel A, and the noncleaved and cleaved fragments of caspase-3 and caspase-8 were detected by Western blot analysis. (C) 293/ACE2 cells grown on coverslips were infected with SARS-CoV as described for panel A and subjected to immunofluorescence analysis using rabbit antiserum directed against the nucleoprotein of SARS-CoV (N) (red). DAPI (4′,6′-diamidino-2-phenylindole) staining (blue) visualizes cell nuclei. Chromatin condensation is indicated by white arrows. (D) 293/ACE2 cells were infected with SARS-CoV as described for panel A; lysed at 8, 24, 48, and 72 h p.i.; and subjected to Western blot analysis with anti-N antiserum. (E) Immunofluorescence analysis of noninfected and SARS-CoV-infected 293/ACE2 cells was performed as described for panel C.

infected cells at 24 h p.i. is most likely due to the activity of cellular eIF2α kinases other than PKR (see below).

Inhibition of PKR expression by PPMO treatment. To investigate the effect of PKR activity on apoptosis and SARS-CoV replication, we employed a knockdown strategy using sequence-specific PPMO. PPMO enter cells readily under standard culturing conditions (2, 17, 39) and are relatively stable in human cells and serum (82). A number of evaluations have indicated that incubation with 10 to 20 μM PPMO was minimally cytotoxic to noninfected cells under conditions similar to those used in our study (19, 39).

Four different PPMO, targeted to different regions of PKR mRNA, were tested for their ability to reduce PKR expression in 293 cells (for PPMO sequences and target locations, see Table 1). As controls for off-target effects, actin levels were monitored and a PPMO of nonsense sequence ("scramble") was included. Initially, 293 cells were incubated with 10 or 20 μM PPMO for 48 h, lysates made, and protein levels visualized by Western blot analysis. As shown in Fig. 3A, treatment with 10 μM of the ex-7 or ex-8 PPMO significantly and specifically reduced the amount of PKR protein in the cells. The reduction was even more pronounced when 20 μM PPMO ex-7 or -8 was used. The "AUG," 5′ED, and "scramble" PPMO had no effect on PKR expression, and actin levels were generally unaffected (Fig. 3A).

RT-PCR was conducted with cellular RNA isolated from PPMO-treated 293 cells to amplify nt 457 to 1850 of human PKR mRNA and thereby produce a PCR fragment of 1,394 nt in length. While treatment of cells with PPMO ex-7 or ex-8 led to synthesis of appropriately shortened PCR fragments, PPMO

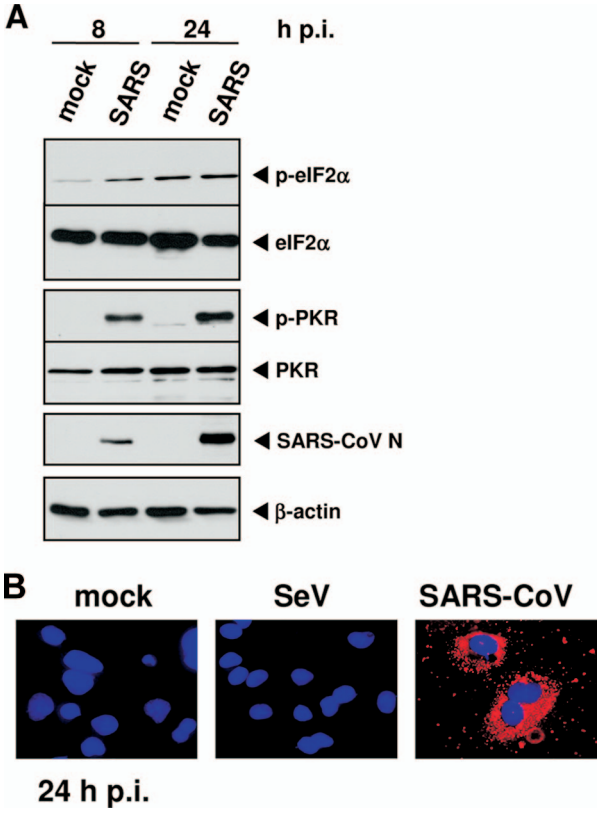

FIG. 2. Phosphorylation of eIF2α and PKR in SARS-CoV-infected 293/ACE2 cells. (A) 293/ACE2 cells were infected with SARS-CoV (MOI, 0.01), and samples harvested at 8 and 24 h p.i. The phosphorylation state of eIF2α and PKR was determined by Western blot analysis using antibodies directed against the respective proteins. Infection of cells was monitored by detecting the SARS-CoV N protein in cell lysates diluted 1 to 100. (B) SARS-CoV- and SeV-infected 293/ACE2 cells were fixed at 24 h p.i. infection and stained with J2 mouse monoclonal antibody (1:100), specifically recognizing dsRNA (red). DAPI staining (blue) visualizes cell nuclei.

"scramble" did not affect the PCR fragment size (Fig. 3B). Sequence analysis of the different PCR fragments of human PKR mRNA revealed a deletion of nt 952 to 1028 in PCR fragment "ex-7" and a deletion of nt 950 to 1116 in PCR fragment "ex-8." PCR fragment "scramble" was identical in sequence to the corresponding region of the GenBank-annotated PKR mRNA. These results confirm that the ex-7 and ex-8 PPMO interfered with splicing events at the intended locations, presumably by disrupting spliceosome assembly on the PKR pre-mRNA through steric interference (1). PPMO targeted to protein-coding sequence located well downstream from the AUG initiator are unlikely to be effective at interfering with translation (67). However, because the ex-7 and -8 PPMO target sequences are present in the mature mRNA, it is possible that these PPMO also reduced the translation of PKR mRNA.

Gene expression knockdown using small interfering RNAs can induce a type I IFN response (36, 56). To explore whether treatment of cells with PPMO would similarly lead to IFN induction, reporter gene assays were performed. Cells were transfected with the pHISG-54 reporter plasmid, which contains the firefly luciferase gene under the control of the IFN-stimulated response element region of the human IFN-stimulated gene ISG-54, along with the expression plasmid pRL-SV40, which constitutively expresses *Renilla* luciferase. Twenty-four hours later, the cells were either treated with 20 μM PPMO or infected with SeV to induce ISG-54-activity for 48 h before reporter gene assays. The results show that PPMO 5′ED, ex-7, and ex-8 did not induce a type I IFN response (Fig. 3C). PPMO "AUG" treatment produced a slight increase in reporter gene activity, but since this PPMO did not produce significant downregulation of PKR expression anyway, it was not used further in this study.

Next, we investigated the kinetics of PPMO-mediated inhibition of PKR expression. 293 cells were treated with various PPMO and harvested at different time points posttreatment. PKR expression was determined by analysis of Western blots and quantified by normalizing PKR bands to corresponding actin bands. Figure 3D shows that 72 h of treatment with PPMO ex-8 caused a profound reduction in PKR expression. PPMO ex-7 treatment likewise reduced PKR expression markedly; however, the somewhat reduced actin signal indicated that it may have also caused cytopathic effects (Fig. 3A and D). Therefore, only PPMO ex-8 was used for further studies.

The experiment described above was repeated using 293/ACE2 cells instead of 293 cells, and similar profiles of PPMO-mediated downregulation of PKR and actin expression were obtained (see below). Attempts to inhibit PKR expression in Vero cells failed, probably due to sequence differences between human and simian PKR genes (data not shown). In summary, treatment with PPMO ex-8 effectively and specifically inhibited PKR expression in human 293 and 293/ACE2 cells.

Inhibition of PKR in SARS-CoV-infected cells does not affect viral replication. We sought to explore the impact of PKR activation on SARS-CoV growth. 293/ACE2 cells were treated with 20 μM of various PPMO for 72 h and then infected with SARS-CoV at a low MOI. Supernatants were harvested 48 h later, and virus titers were determined by $TCID_{50}$ assays. Surprisingly, neither SARS-CoV nucleoprotein expression nor replication efficiency was affected by ex-8 PPMO treatment compared to that in infected cells that were mock treated, indicating that SARS-CoV is not sensitive to the antiviral effects of activated PKR in 293/ACE2 cells (Fig. 4A and B). Although the viral titer of ex-8- or mock-treated cells was about 1 $\log_{10}$ unit higher than titers of 5′ED- or "scramble"-treated cells, this difference was calculated to be not significant (Student's t test, $P > 0.100$).

To determine if SARS-CoV-induced apoptosis was potentially mediated by PKR, infected-cell lysates receiving various treatments were harvested at 48 h p.i. and analyzed for PKR expression and PARP cleavage. As shown in Fig. 4B, cells treated with the ex-8 PPMO displayed no PKR expression, as expected from the above results. PARP cleavage occurred in SARS-CoV-infected cells that were either mock treated or treated with the "scramble" or 5′ED PPMO. However, in SARS-CoV-infected cells treated with the ex-8 PPMO, PARP cleavage was strongly reduced compared to controls, indicating that the induction of apoptosis was impaired in these cells. The amount of phosphorylated eIF2α was also analyzed and found to be high in all samples, irrespective of whether the cells were

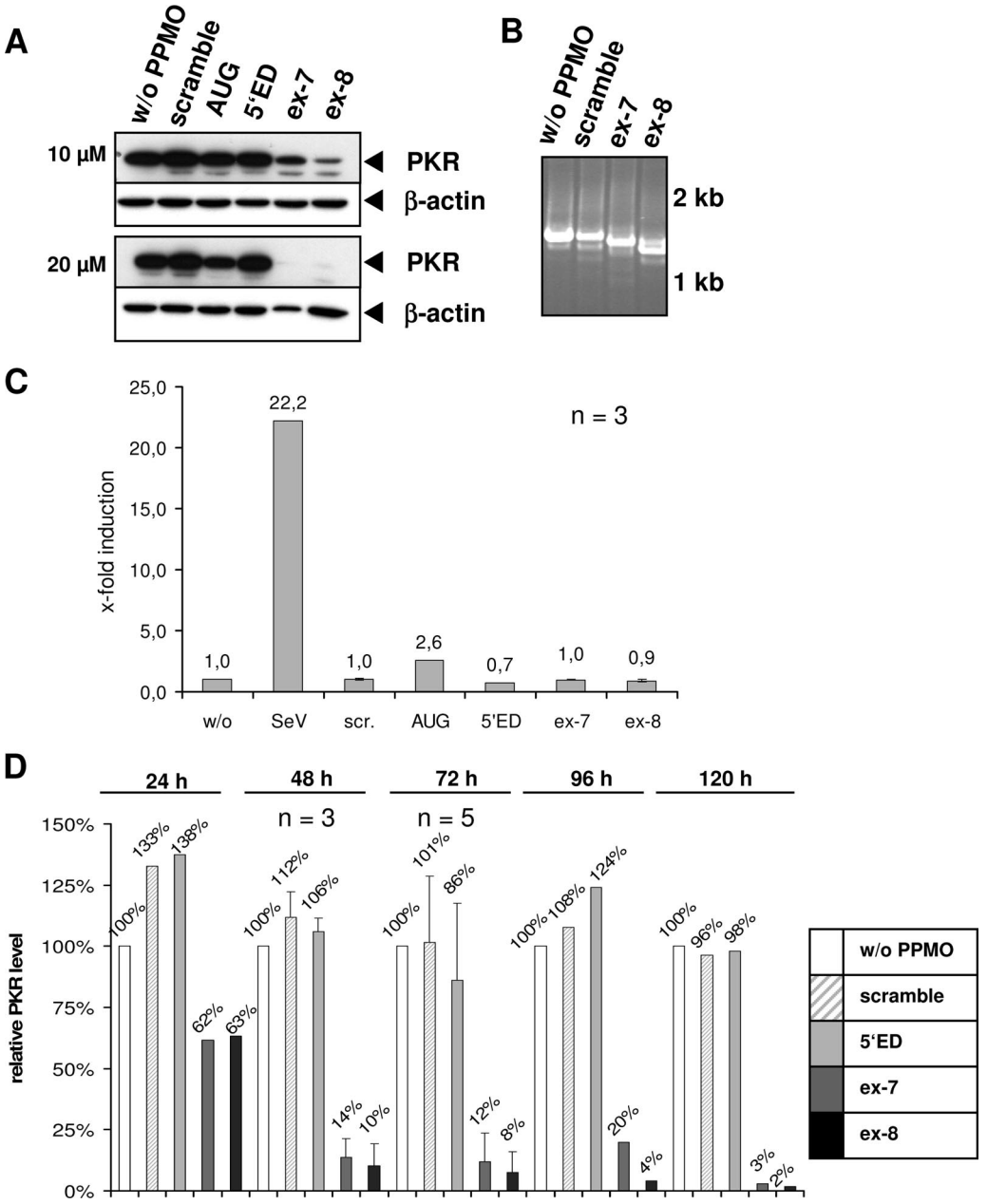

FIG. 3. Inhibition of PKR expression with PPMO. (A) 293 cells were treated with 10 or 20 μM of the indicated PPMO (see Table 1 for a description of PPMO sequences and targets) or left untreated (w/o PPMO) for 48 h, and cell lysates were then analyzed on Western blots with anti-PKR and antiactin antibodies. (B) Total cellular RNA was isolated from 293 cells treated with 20 μM of indicated PPMO for 48 h. RNA was analyzed by RT-PCR using primers designed to amplify a PKR mRNA fragment of 1,394 bases. (C) 293 cells were transfected with two reporter plasmids, pHISG-54-Luc (firefly luciferase gene under the control of an IFN-inducible promoter) and pRL-SV40 (produces *Renilla* luciferase). At 24 h posttransfection, cells were either infected with SeV (20 hemagglutinating units) or mock or 20 μM PPMO treated for an additional 48 h. Cell lysates were assayed by using a dual luciferase system, and relative firefly luciferase activity was normalized to *Renilla* luciferase activities as a standard of transfection efficiency. The experiment was performed in triplicate, and standard deviations are shown. (D) Lysates of 20 μM PPMO-treated or untreated 293 cells were analyzed over time (24 h to 120 h) for levels of PKR expression by Western blot analysis. PKR levels were quantified by densitometry and normalized to corresponding actin bands. The amount of PKR in each sample compared to the mock-treated control is shown as a percentage above each bar of the graph. Because of limited PPMO availability, this assay was performed only twice at some of the time points. The 48-h and 72-h values were determined three to five times.

infected or not and without any correlation to PKR expression (Fig. 4B). We assume that the high background phosphorylation of eIF2α at 48 h p.i. was due to the activity of eIF2α kinases other than PKR, which were induced by the high cell density characteristic of this time point (59).

Together, the results shown in Fig. 4 indicate that although PKR mediates the induction of apoptosis in SARS-CoV-infected cells, neither PKR nor apoptosis has a major effect on virus growth for up to 72 h p.i. in cultured 293/ACE2 cells.

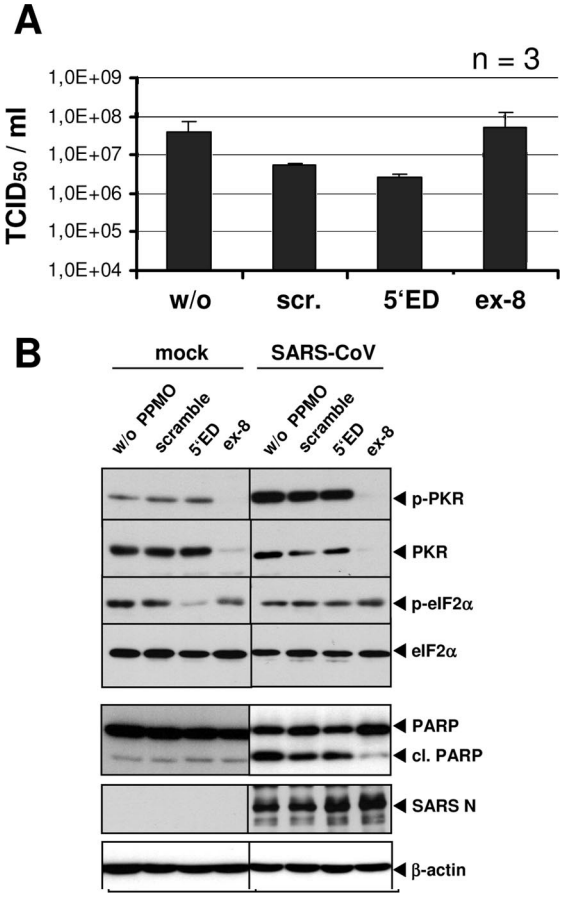

FIG. 4. Inhibition of PKR expression with PPMO does not affect SARS-CoV replication. (A) A total of 4×10^4 293/ACE2 cells were treated with 20 μM of indicated PPMO for 72 h and then infected with SARS-CoV (MOI, 0.01). After removal of the inoculum, DMEM with 2% FCS containing 20 μM of the same PPMO was added to the cells. At 48 h p.i., cells were harvested and supernatants were used for $TCID_{50}$ assays. This experiment was performed in triplicate, and standard deviations are shown. Student's *t* test revealed no statistical significance ($P > 0.100$) to the slight differences in viral titers among samples. (B) Cell lysates were subjected to Western blot analysis by using anti-phospho-PKR (pT446) (panel 1 from top), anti-PKR (panel 2), anti-phospho-eIF2α (Ser51) (panel 3), anti-eIF2α (panel 4), anti-PARP (panel 5), anti-SARS-CoV-N (panel 6), and anti-β-actin (panel 7) antibodies. The experiment was performed three times with similar outcome. w/o, without PPMO.

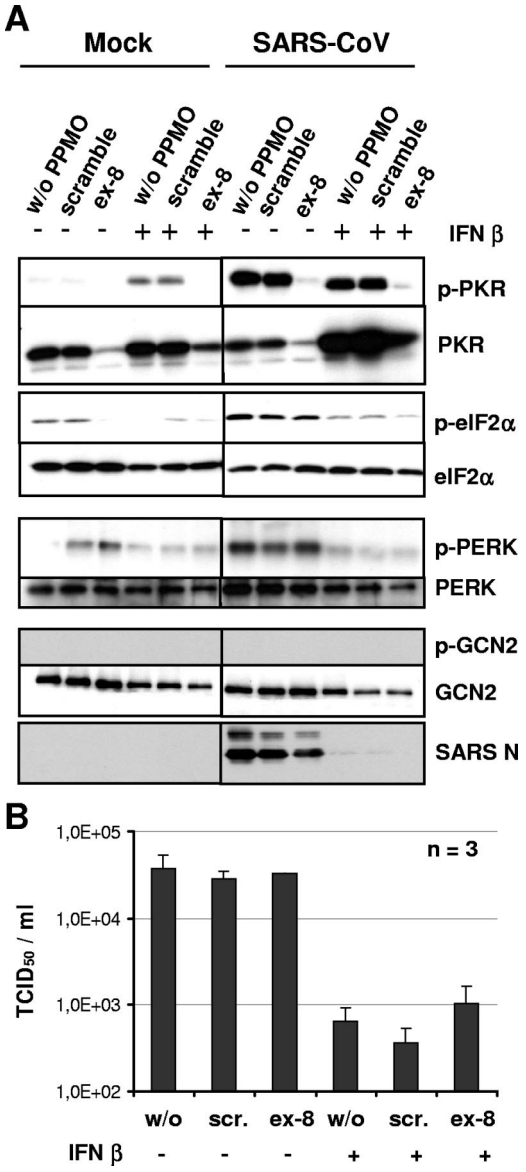

FIG. 5. Inhibition of IFN-β-induced PKR expression by PPMO does not affect SARS-CoV replication. (A) A total 4×10^4 293/ACE2 cells were treated with the indicated PPMO for 72 h and then with (+) or without (−) 10,000 IU of IFN-β for 24 h before infection with SARS-CoV at an MOI of 0.01. After the inoculum was removed, DMEM with 2% FCS and without or with 20 μM of the indicated PPMO was added to the cells. At 24 h p.i., cells were harvested and subjected to SDS-polyacrylamide gel electrophoresis. The levels of phosphorylated and total PKR (panel 1 from top), phosphorylated and total eIF2α (panel 2), phosphorylated and total PERK (panel 3), phosphorylated and total GCN2 (panel 4), and SARS-CoV nucleoprotein were determined by Western blot analysis. (B) Virus titers were determined by $TCID_{50}$ assays. Standard deviations are shown. Student's *t* test revealed that the viral titer differences between samples receiving IFN-β-treatment were not statistically significant ($P > 0.100$). The experiments were performed three times with similar outcomes.

Knockdown of PKR does not diminish the antiviral effect of IFN-β. SARS-CoV is known to be sensitive to IFN-β treatment (62). Since PKR is a major antiviral factor known to be upregulated by type I IFNs, we investigated the contribution of PKR to the antiviral effects of IFN-β against SARS-CoV. 293/ACE2 cells were first treated with PPMO and then incubated with IFN-β and subsequently infected with SARS-CoV. At 24 h p.i. lysates of cells were analyzed for total and phosphorylated PKR and eIF2α. Figure 5A shows that PKR expression was strongly upregulated in cells which were both IFN-β treated and SARS-CoV infected. Upregulation of PKR was less pronounced in IFN-β-treated cells which were not infected. Importantly, however, PPMO ex-8 treatment reduced PKR expression, even when IFN-β was simultaneously present. Phosphorylated PKR was barely detectable in either noninfected or SARS-CoV-infected cells treated with ex-8 PPMO (Fig. 5A, top panel). Moderate PKR phosphorylation was observed in noninfected cells treated with IFN-β. In SARS-CoV-infected cells that were not treated with ex-8

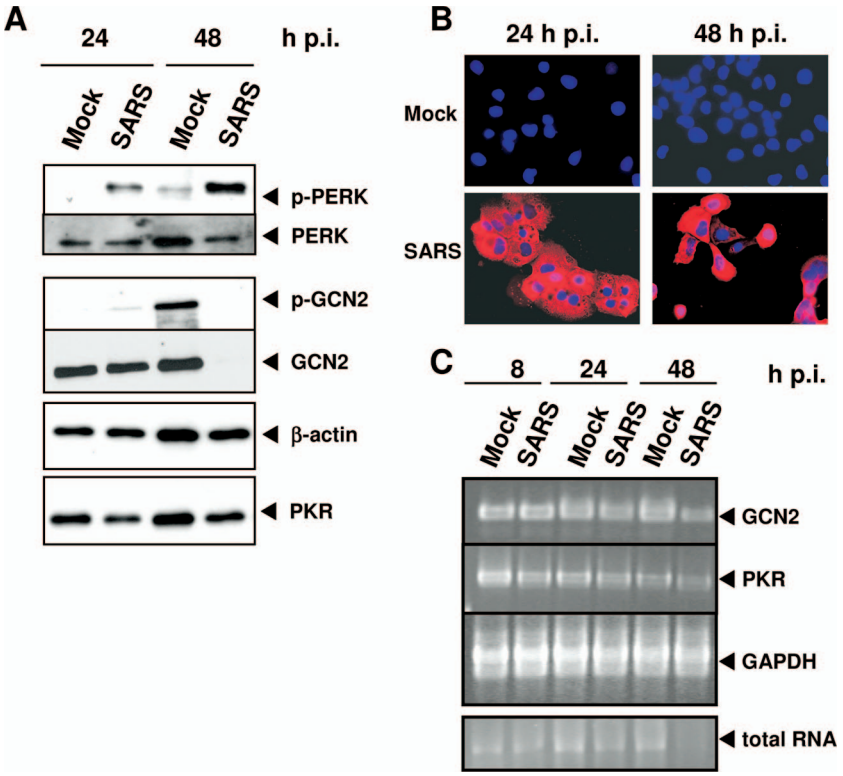

FIG. 6. Induction of eIF2α-phosphorylating kinases during SARS-CoV infection. (A) 293/ACE2 cells were infected with SARS-CoV at an MOI of 0.01 and lysed at 24 h and 48 h p.i. Western blot analysis was performed with antibodies against β-actin and the phosphorylated (p) and nonphosphorylated forms of PERK, GCN2, and PKR. This experiment was repeated three times with similar outcomes. (B) 293/ACE2 cells grown on coverslips were infected with SARS-CoV as described for panel A. Immunofluorescence analysis using rabbit antiserum directed against the nucleoprotein of SARS-CoV (N) (red) revealed that 100% of the cells were infected. DAPI staining (blue) was performed to visualize cell nuclei. (C) Total RNA of 293/ACE2 cells infected with SARS-CoV as described for panel A was isolated at 8, 24, or 48 h p.i., and 5 μl of each RNA sample was subjected to RT-PCR analyses to determine GCN2-, PKR-, and GAPDH-specific mRNA levels (30 cycles). In addition, 1 μl of each total cellular RNA sample was analyzed by agarose gel electrophoresis. The 18S rRNA band is shown and indicates the amount of total cellular RNA.

PPMO, PKR phosphorylation was strongly induced irrespective of whether the cells were treated with IFN-β or not. Interestingly, the phosphorylation pattern of eIF2α was not consistent with that of PKR phosphorylation (Fig. 5A). Compared to that in nontreated cells, eIF2α phosphorylation was reduced in cells treated with IFN-β and did not correlate with PKR phosphorylation. These data clearly indicate that kinases other than PKR are involved in SARS-CoV-induced eIF2α phosphorylation. We therefore analyzed the phosphorylation state of PERK and GCN2, the two other kinases known to phosphorylate eIF2α in response to viral infections. Indeed, PERK was phosphorylated in SARS-CoV-infected cells, but only if the cells were not additionally treated with IFN-β. Moreover, the total amount of PERK was reduced after IFN-β treatment (Fig. 5A). In contrast to PERK, GCN2 was not phosphorylated in SARS-CoV-infected cells (Fig. 5A). These data indicate that eIF2α phosphorylation correlates with activated PERK in infected cells, suggesting that PERK mediates phosphorylation of eIF2α in SARS-CoV-infected cells.

$TCID_{50}$ assays revealed that IFN-β treatment of infected cells reduced viral titers by about 2 $\log_{10}$ units (Fig. 5B). Downregulation of PKR by the ex-8 PPMO, however, did not significantly affect viral titers (Student's t test, $P > 0.100$), confirming that active PKR has no important effect on SARS-CoV replication. As expected, expression of SARS-CoV N protein was dramatically diminished in IFN-β-treated cells (Fig. 5A).

Induction of eIF2α kinases in SARS-CoV-infected cells. We also examined the expression and phosphorylation state of GCN2 and PERK late in infection, i.e., at a time when apoptosis is observable. 293/ACE2 cells were infected with SARS-CoV, and GCN2 and PERK were then detected by Western blot analysis in samples taken at 24 h or 48 h pi. (Fig. 6A). In parallel, the efficiency of virus infection was determined by immunofluorescence analysis (Fig. 6B). Increased PERK phosphorylation was observed in infected cells at 24 h and 48 h p.i. (Fig. 6A). In contrast, GCN2 was not phosphorylated in SARS-CoV-infected cells late in infection (Fig. 6A). Oddly, GCN2 was found to be phosphorylated in noninfected cells at 48 h p.i., perhaps due to amino acid deprivation in the cells. Interestingly, the amount of GCN2 was drastically reduced in SARS-CoV-infected cells at 48 h p.i., whereas the levels of actin and PKR were only slightly affected (Fig. 6A). Thus, we conclude that the level of GCN2 protein is actively downregulated in SARS-CoV-infected cells. To analyze whether reduced GCN2 protein levels were due to decreased transcription or stability of GCN2 mRNA, RT-PCR analyses of GCN2, PKR, and GAPDH mRNAs were performed. Our results revealed that reduction of the GCN2 protein level did not correlate with

degradation of GCN2 mRNA in infected cells. The reduction of GCN2, PKR, and GAPDH mRNAs after 24 and 48 h p.i. likely resulted from the reduced amount of total cellular RNA in SARS-CoV-infected cells, as shown by examination of total RNA by agarose gel electrophoresis (Fig. 6C).

DISCUSSION

The aim of this study was to investigate the role of the antiviral protein PKR in SARS-CoV-infected cells. We found that both PKR and its substrate eIF2α are phosphorylated in SARS-CoV-infected cells. When PKR expression was downregulated with antisense PPMO, PARP cleavage was strongly reduced in infected cells, whereas eIF2α was still phosphorylated. Strikingly, viral replication was not enhanced when PKR was knocked down, indicating that SARS-CoV is not sensitive to the antiviral activities of PKR.

Phosphorylation of eIF2α at Ser51 is one important mechanism by which cells restrict translation, and it may contribute to the induction of apoptosis (29). So far, four cellular kinases are known to phosphorylate eIF2α, and three of those, PKR, PERK, and GCN2, can be activated upon virus-induced stress (3, 5, 11, 45, 74). At the beginning of our study, several lines of evidence pointed to PKR as the most promising candidate to phosphorylate eIF2α in SARS-CoV-infected cells. First, the PKR activator dsRNA is present in large amounts in SARS-CoV-infected cells (Fig. 2B) (76). Second, eIF2α and PKR phosphorylation profiles were similar to each other in SARS-CoV-infected cells (Fig. 2). Third, PKR is known to play a prominent role in host antiviral defense, and many viruses have evolved countermeasures to overcome its function (24, 25). Our results indicate that SARS-CoV also employs a strategy to counteract the antiviral effects of PKR. Most likely, rather than inhibiting PKR activation, translation of SARS-CoV mRNAs proceeds despite eIF2α phosphorylation.

Attempts to knock down PKR expression in human cells with conventional approaches, including RNA interference and transfection of known viral PKR inhibitors, were not efficient in our hands. We therefore tested PPMO targeting the PKR mRNA for their ability to block PKR expression. PPMO designed to duplex with viral RNA have been used to inhibit the replication of a number of RNA viruses (reviewed in reference 64), including SARS-CoV (50). In addition, PPMO have been shown to affect eukaryotic gene expression by targeting cellular mRNAs (18, 43, 44). PPMO enter cells by endocytic processes (2), and consequently, no additional reagents or transfection procedures are required for their delivery into cells.

Transient and stable knockdown of PKR in human cells by RNA interference has been described by different groups, with levels of reduction varying between 50% and 98% (20, 23, 40, 86). PKR-deficient HeLa cells showed lower levels of dsRNA-induced apoptosis and impaired phosphorylation of eIF2α (86). When PKR-deficient HeLa cells were infected with E3L-deficient vaccinia virus, eIF2α phosphorylation and apoptosis were impaired, suggesting that eIF2α phosphorylation in vaccinia virus-infected cells is mediated predominantly by PKR (84). However, this seems not to be the case for SARS-CoV, as eIF2α phosphorylation was independent of PKR protein expression.

eIF2α-independent PKR-mediated induction of apoptosis has previously been proposed (30). Although it is known that several effector proteins other than eIF2α, such as NFκB, ATF-3, FADD, and caspase-8, are involved in PKR-mediated apoptosis, the mechanistic details of how PKR induces apoptosis are not fully understood (21). In this study, caspase-8 was activated in SARS-CoV-infected 293/ACE2 cells (Fig. 1), thus supporting the hypothesis that SARS-CoV-triggered apoptosis is mediated by PKR. A recent report by Zhang and Samuel (85), investigating PKR-dependent IRF-3 activation in vaccinia virus-infected cells, provided clear evidence that although small amounts of phosphorylated eIF2α were detectable, knockdown of PKR inhibited the induction of apoptosis.

We hypothesized that since downregulation of PKR in SARS-CoV-infected cells did not lead to inhibition of eIF2α phosphorylation, PERK and/or GCN2 may be activated. It is known that the spike (S) protein of SARS-CoV induces ER stress, leading to activation of cellular unfolded protein response (UPR) pathways (11, 74). SARS-CoV S protein also induces upregulation of the ER chaperones glucose-related proteins 78 and 94 through activation of PERK (11). To date, three different UPR signaling pathways have been identified. They are mediated by the proximal sensor proteins activating transcription factor 6, inositol-requiring protein 1, and PERK (58). Our data indicate that PERK contributes to eIF2α phosphorylation in SARS-CoV-infected cells, whereas GCN2 does not. In contrast to the case for PKR, activation of PERK in SARS-CoV-infected 293/ACE2 cells does not lead to apoptosis. This is in line with the observation that SARS-CoV S protein does not modulate inositol-requiring protein 1 and activating transcription factor 6 signaling pathways and causes only mild induction of the proapoptotic mediator C/EBP-homologous protein, a downstream target of PERK (11). Although understanding of UPR-induced apoptosis is quite limited, it appears that PERK signaling is generally protective, as loss of PERK-mediated eIF2α phosphorylation was associated with reduced survival of cells exposed to ER stress (26, 58).

Among the CoVs, modulation of UPR is not unique to SARS-CoV and has also been described for mouse hepatitis virus (MHV) (4, 9). eIF2α phosphorylation by both PERK and PKR has also been observed in VSV-infected cells. Both PERK and PKR are considered to play crucial roles in host resistance against VSV infection, and activated PERK has been shown to inhibit VSV-induced apoptosis (3, 66). Interestingly, PKR activation seems to be defective in PERK knockout mouse embryonic fibroblasts, indicating a functional cross talk between PERK and PKR (3).

Our data show that both PKR and PERK are activated by SARS-CoV, leading to sustained phosphorylation of eIF2α. It is unclear if SARS-CoV has evolved a strategy to overcome the antiviral activity of PKR or if it utilizes activated PKR as a means to phosphorylate eIF2α, thus imposing a virus-favorable regulatory effect on the cellular translation machinery. Interestingly, IFN-β treatment of SARS-CoV-infected cells not only decreased N protein expression and viral titer but also led to marked reductions of both PERK activation and eIF2α phosphorylation (Fig. 5). These data suggest that virus protein accumulation was too low to induce PERK phosphorylation in IFN-treated cells. However, it is also possible that PERK activation is beneficial for virus replication, a notion that may be

worthy of more detailed investigation in further studies. It would also be interesting to use nonphosphorylatable eIF2α mutants to investigate the role of eIF2α in SARS-CoV propagation in cell culture. However, to our knowledge there are currently no cell lines available that both provide stable expression of nonphosphorylatable eIF2α and permit productive replication of SARS-CoV. It is known that CoVs have evolved various strategies to promote preferential translation of viral mRNAs, including stimulation of viral translation in *cis* by the MHV 5′-leader RNA sequence (69) and the repression of cellular protein synthesis by the SARS-CoV nsp1 protein. SARS-CoV nsp1 specifically induces degradation of host cellular mRNA and inhibits host translation (33). It remains unclear if SARS-CoV replication depends on eIF2α phosphorylation.

Since the inhibitory effects of SARS CoV nsp1 lead to downregulation of the innate immune response, this protein is considered to be an important virulence factor (49, 75). The reported suppression of host gene expression in SARS-CoV-infected cells is consistent with our observation that GCN2 is dramatically downregulated during late stages of infection (Fig. 6). Interestingly, RT-PCR analyses revealed that the reduced level of GCN2 protein in SARS-CoV-infected cells is not the result of specific degradation of GCN2 mRNA. Further studies addressing protein stability may help to clarify how SARS-CoV infection leads to GCN2 downregulation.

SARS-CoV-induced cell death during late stages of infection has been observed in cell culture studies (60). Although many SARS-CoV proteins have been shown to be potent inducers of apoptosis when expressed in cells (10, 35, 70, 72, 83), there is limited knowledge about exactly how apoptosis is induced. Studies of persistently infected Vero E6 cells revealed that SARS-CoV modulates the phosphatidylinositol 3-kinase-Akt pathway, leading to Akt phosphorylation early in infection (46). A number of RNA viruses activate the phosphatidylinositol 3-kinase-Akt prosurvival pathway during the initial stages of infection and eventually induce apoptosis later in infection, facilitating virus spread (46). However, when SARS-CoV-induced apoptosis was inhibited either by caspase inhibitors or by overexpression of the antiapoptotic Bcl-2 protein, virus replication was not affected, indicating that apoptosis is not needed for efficient virus release (8, 55). These observations are in line with our results demonstrating that downregulation of PKR led to inhibition of apoptosis without affecting viral titers (Fig. 5). In addition, further analyses using the caspase-specific inhibitor zVAD-fmk showed that apoptosis does not affect propagation of SARS-CoV in cell culture under the conditions of this study (data not shown).

Induction of cell death by MHV and transmissible porcine gastroenteritis virus has been intensively studied (71). It is known that infection of oligodendrocytes with MHV triggers apoptosis during cell entry through the activation of the Fas signaling pathway (42). Later in the MHV infectious cycle, eIF2α becomes phosphorylated (4). However, the impairment of host translation by phosphorylated eIF2α apparently does not contribute to more efficient MHV replication or to the induction of apoptosis (54). Relatively little is known about the induction of apoptosis by human CoVs or about the contribution of eIF2α phosphorylation to the death of infected cells. Among human CoVs, it has been reported that OC43 and 229E induce apoptosis in murine neuronal cells (32) and in monocytes and macrophages (16), respectively.

In summary, we have demonstrated that SARS-CoV activates both PKR and PERK and that these events lead to sustained phosphorylation of eIF2α in infected cells. Interestingly, virus replication seems to remain unimpaired by eIF2α phosphorylation, and we hypothesize that, in contrast, eIF2α phosphorylation may instead promote the SARS-CoV infectious cycle by contributing to the suppression of host translation.

ACKNOWLEDGMENTS

We thank S. Makino, UTMB, Galveston, TX, for generously providing 293/ACE2 cells; L. Martínez-Sobrido and A. Garcia-Sastre, Mount Sinai School of Medicine, New York, for the SARS-CoV antibody; C. F. Basler, Mount Sinai School of Medicine, New York, for providing Sendai virus strain Cantell; W. J. Neubert, Max Planck Institute, Martinsried, for the Sendai virus antibody; D. Levy, New York University School of Medicine, New York, for plasmid pHISG-54-Luc; and the Chemistry Group at AVI BioPharma for the production of PPMO.

This work was supported by DFG grant Mu1365/1-1, by the Sino-German Center for Science Promotion, and by SFB 535.

REFERENCES

1. **Aartsma-Rus, A., and G. J. van Ommen.** 2007. Antisense-mediated exon skipping: a versatile tool with therapeutic and research applications. RNA **13:**1609–1624.
2. **Abes, S., H. M. Moulton, P. Clair, P. Prevot, D. S. Youngblood, R. P. Wu, P. L. Iversen, and B. Lebleu.** 2006. Vectorization of morpholino oligomers by the (R-Ahx-R)4 peptide allows efficient splicing correction in the absence of endosomolytic agents. J. Control Release **116:**304–313.
3. **Baltzis, D., L. K. Qu, S. Papadopoulou, J. D. Blais, J. C. Bell, N. Sonenberg, and A. E. Koromilas.** 2004. Resistance to vesicular stomatitis virus infection requires a functional cross talk between the eukaryotic translation initiation factor 2α kinases PERK and PKR. J. Virol. **78:**12747–12761.
4. **Bechill, J., Z. Chen, J. W. Brewer, and S. C. Baker.** 2008. Coronavirus infection modulates the unfolded protein response and mediates sustained translational repression. J. Virol. **82:**4492–4501.
5. **Berlanga, J. J., I. Ventoso, H. P. Harding, J. Deng, D. Ron, N. Sonenberg, L. Carrasco, and C. de Haro.** 2006. Antiviral effect of the mammalian translation initiation factor 2alpha kinase GCN2 against RNA viruses. EMBO J. **25:**1730–1740.
6. **Bitzer, M., F. Prinz, M. Bauer, M. Spiegel, W. J. Neubert, M. Gregor, K. Schulze-Osthoff, and U. Lauer.** 1999. Sendai virus infection induces apoptosis through activation of caspase-8 (FLICE) and caspase-3 (CPP32). J. Virol. **73:**702–708.
7. **Boehmann, Y., S. Enterlein, A. Randolf, and E. Muhlberger.** 2005. A reconstituted replication and transcription system for Ebola virus Reston and comparison with Ebola virus Zaire. Virology **332:**406–417.
8. **Bordi, L., C. Castilletti, L. Falasca, F. Ciccosanti, S. Calcaterra, G. Rozera, A. Di Caro, S. Zaniratti, A. Rinaldi, G. Ippolito, M. Piacentini, and M. R. Capobianchi.** 2006. Bcl-2 inhibits the caspase-dependent apoptosis induced by SARS-CoV without affecting virus replication kinetics. Arch. Virol. **151:** 369–377.
9. **Boyce, M., K. F. Bryant, C. Jousse, K. Long, H. P. Harding, D. Scheuner, R. J. Kaufman, D. Ma, D. M. Coen, D. Ron, and J. Yuan.** 2005. A selective inhibitor of eIF2alpha dephosphorylation protects cells from ER stress. Science **307:**935–939.
10. **Chan, C. M., C. W. Ma, W. Y. Chan, and H. Y. Chan.** 2007. The SARS-coronavirus membrane protein induces apoptosis through modulating the Akt survival pathway. Arch. Biochem. Biophys. **459:**197–207.
11. **Chan, C. P., K. L. Siu, K. T. Chin, K. Y. Yuen, B. Zheng, and D. Y. Jin.** 2006. Modulation of the unfolded protein response by the severe acute respiratory syndrome coronavirus spike protein. J. Virol. **80:**9279–9287.
12. **Chen, J., Y. Q. Xie, H. T. Zhang, J. W. Wan, D. T. Wang, Z. H. Lu, Q. Z. Wang, X. H. Xue, W. X. Si, Y. F. Luo, and H. M. Qiu.** 2003. Lung pathology of severe acute respiratory syndrome. Zhongguo Yi Xue Ke Xue Yuan Xue Bao **25:**360–362.
13. **Chen, J. J.** 2007. Regulation of protein synthesis by the heme-regulated eIF2alpha kinase: relevance to anemias. Blood **109:**2693–2699.
14. **Chen, J. J., and I. M. London.** 1995. Regulation of protein synthesis by heme-regulated eIF-2 alpha kinase. Trends Biochem. Sci. **20:**105–108.
15. **Clemens, M. J., and A. Elia.** 1997. The double-stranded RNA-dependent protein kinase PKR: structure and function. J. Interferon Cytokine Res. **17:**503–524.

16. **Collins, A. R.** 2002. In vitro detection of apoptosis in monocytes/macrophages infected with human coronavirus. Clin. Diagn. Lab. Immunol. **9:**1392–1395.
17. **Deas, T. S., I. Binduga-Gajewska, M. Tilgner, P. Ren, D. A. Stein, H. M. Moulton, P. L. Iversen, E. B. Kauffman, L. D. Kramer, and P. Y. Shi.** 2005. Inhibition of flavivirus infections by antisense oligomers specifically suppressing viral translation and RNA replication. J. Virol. **79:**4599–4609.
18. **Fletcher, S., K. Honeyman, A. M. Fall, P. L. Harding, R. D. Johnsen, J. P. Steinhaus, H. M. Moulton, P. L. Iversen, and S. D. Wilton.** 2007. Morpholino oligomer-mediated exon skipping averts the onset of dystrophic pathology in the mdx mouse. Mol. Ther. **15:**1587–1592.
19. **Gabriel, G., A. Nordmann, D. A. Stein, P. L. Iversen, and H. D. Klenk.** 2008. Morpholino oligomers targeting the PB1 and NP genes enhance the survival of mice infected with highly pathogenic influenza A H7N7 virus. J. Gen. Virol. **89:**939–948.
20. **Gainey, M. D., P. J. Dillon, K. M. Clark, M. J. Manuse, and G. D. Parks.** 2008. Paramyxovirus-induced shutoff of host and viral protein synthesis: role of the P and V proteins in limiting PKR activation. J. Virol. **82:**828–839.
21. **Garcia, M. A., E. F. Meurs, and M. Esteban.** 2007. The dsRNA protein kinase PKR: virus and cell control. Biochimie **89:**799–811.
22. **Gil, J., J. Alcami, and M. Esteban.** 1999. Induction of apoptosis by double-stranded-RNA-dependent protein kinase (PKR) involves the alpha subunit of eukaryotic translation initiation factor 2 and NF-κB. Mol. Cell. Biol. **19:**4653–4663.
23. **Gilfoy, F. D., and P. W. Mason.** 2007. West Nile virus-induced interferon production is mediated by the double-stranded RNA-dependent protein kinase PKR. J. Virol. **81:**11148–11158.
24. **Grandvaux, N., B. R. tenOever, M. J. Servant, and J. Hiscott.** 2002. The interferon antiviral response: from viral invasion to evasion. Curr. Opin. Infect. Dis. **15:**259–267.
25. **Haller, O., G. Kochs, and F. Weber.** 2006. The interferon response circuit: induction and suppression by pathogenic viruses. Virology **344:**119–130.
26. **Harding, H. P., Y. Zhang, A. Bertolotti, H. Zeng, and D. Ron.** 2000. Perk is essential for translational regulation and cell survival during the unfolded protein response. Mol. Cell **5:**897–904.
27. **He, B.** 2006. Viruses, endoplasmic reticulum stress, and interferon responses. Cell Death Differ. **13:**393–403.
28. **Hierholzer, J. C., and R. A. Killington.** 1996. Virus isolation and quantitation, p. 36–38. *In* B. W. J. Mahy and H. O. Kangro (ed.), Virology methods manual. Academic Press Limited, London, United Kingdom.
29. **Holcik, M., and N. Sonenberg.** 2005. Translational control in stress and apoptosis. Nat. Rev. Mol. Cell Biol. **6:**318–327.
30. **Hsu, L. C., J. M. Park, K. Zhang, J. L. Luo, S. Maeda, R. J. Kaufman, L. Eckmann, D. G. Guiney, and M. Karin.** 2004. The protein kinase PKR is required for macrophage apoptosis after activation of Toll-like receptor 4. Nature **428:**341–345.
31. **Ivana Scovassi, A., and M. Diederich.** 2004. Modulation of poly(ADP-ribosylation) in apoptotic cells. Biochem. Pharmacol. **68:**1041–1047.
32. **Jacomy, H., and P. J. Talbot.** 2006. HCoV-OC43-induced apoptosis of murine neuronal cells. Adv. Exp. Med. Biol. **581:**473–478.
33. **Kamitani, W., K. Narayanan, C. Huang, K. Lokugamage, T. Ikegami, N. Ito, H. Kubo, and S. Makino.** 2006. Severe acute respiratory syndrome coronavirus nsp1 protein suppresses host gene expression by promoting host mRNA degradation. Proc. Natl. Acad. Sci. USA **103:**12885–12890.
34. **Kaufman, R. J.** 1999. Double-stranded RNA-activated protein kinase mediates virus-induced apoptosis: a new role for an old actor. Proc. Natl. Acad. Sci. USA **96:**11693–11695.
35. **Khan, S., B. C. Fielding, T. H. Tan, C. F. Chou, S. Shen, S. G. Lim, W. Hong, and Y. J. Tan.** 2006. Over-expression of severe acute respiratory syndrome coronavirus 3b protein induces both apoptosis and necrosis in Vero E6 cells. Virus Res. **122:**20–27.
36. **Kim, J. Y., S. Choung, E. J. Lee, Y. J. Kim, and Y. C. Choi.** 2007. Immune activation by siRNA/liposome complexes in mice is sequence-independent: lack of a role for Toll-like receptor 3 signaling. Mol. Cells **24:**247–254.
37. **Ksiazek, T. G., D. Erdman, C. S. Goldsmith, S. R. Zaki, T. Peret, S. Emery, S. Tong, C. Urbani, J. A. Comer, W. Lim, P. E. Rollin, S. F. Dowell, A. E. Ling, C. D. Humphrey, W. J. Shieh, J. Guarner, C. D. Paddock, P. Rota, B. Fields, J. DeRisi, J. Y. Yang, N. Cox, J. M. Hughes, J. W. LeDuc, W. J. Bellini, and L. J. Anderson.** 2003. A novel coronavirus associated with severe acute respiratory syndrome. N. Engl. J. Med. **348:**1953–1966.
38. **Lai, M. M. C., and K. V. Holmes.** 2001. *Coronaviridae*: the viruses and their replication, p. 1163–1185. *In* D. M. Knipe, P. M. Howley, D. E. Griffin, R. A. Lamb, M. A. Martin, B. roizman, and S. E. Straus (ed.), Fields virology, 4th ed. Lippincott Williams & Wilkins, Philadelphia, PA.
39. **Lai, S. H., D. A. Stein, A. Guerrero-Plata, S. L. Liao, T. Ivanciuc, C. Hong, P. L. Iversen, A. Casola, and R. P. Garofalo.** 2008. Inhibition of respiratory syncytial virus infections with morpholino oligomers in cell cultures and in mice. Mol. Ther. **16:**1120–1128.
40. **Lee, E. S., C. H. Yoon, Y. S. Kim, and Y. S. Bae.** 2007. The double-strand RNA-dependent protein kinase PKR plays a significant role in a sustained ER stress-induced apoptosis. FEBS Lett. **581:**4325–4332.
41. **Licata, J. M., and R. N. Harty.** 2003. Rhabdoviruses and apoptosis. Int. Rev. Immunol. **22:**451–476.
42. **Liu, Y., and X. Zhang.** 2007. Murine coronavirus-induced oligodendrocyte apoptosis is mediated through the activation of the Fas signaling pathway. Virology **360:**364–375.
43. **Marshall, N. B., S. K. Oda, C. A. London, H. M. Moulton, P. L. Iversen, N. I. Kerkvliet, and D. V. Mourich.** 2007. Arginine-rich cell-penetrating peptides facilitate delivery of antisense oligomers into murine leukocytes and alter pre-mRNA splicing. J. Immunol. Methods **325:**114–126.
44. **McClorey, G., A. M. Fall, H. M. Moulton, P. L. Iversen, J. E. Rasko, M. Ryan, S. Fletcher, and S. D. Wilton.** 2006. Induced dystrophin exon skipping in human muscle explants. Neuromuscul. Disord. **16:**583–590.
45. **Medigeshi, G. R., A. M. Lancaster, A. J. Hirsch, T. Briese, W. I. Lipkin, V. Defilippis, K. Fruh, P. W. Mason, J. Nikolich-Zugich, and J. A. Nelson.** 2007. West Nile virus infection activates the unfolded protein response, leading to CHOP induction and apoptosis. J. Virol. **81:**10849–10860.
46. **Mizutani, T., S. Fukushi, M. Saijo, I. Kurane, and S. Morikawa.** 2004. Importance of Akt signaling pathway for apoptosis in SARS-CoV-infected Vero E6 cells. Virology **327:**169–174.
47. **Mizutani, T., S. Fukushi, M. Saijo, I. Kurane, and S. Morikawa.** 2004. Phosphorylation of p38 MAPK and its downstream targets in SARS coronavirus-infected cells. Biochem. Biophys. Res. Commun. **319:**1228–1234.
48. **Nallagatla, S. R., J. Hwang, R. Toroney, X. Zheng, C. E. Cameron, and P. C. Bevilacqua.** 2007. 5′-triphosphate-dependent activation of PKR by RNAs with short stem-loops. Science **318:**1455–1458.
49. **Narayanan, K., C. Huang, K. Lokugamage, W. Kamitani, T. Ikegami, C. T. Tseng, and S. Makino.** 2008. Severe acute respiratory syndrome coronavirus nsp1 suppresses host gene expression, including that of type I interferon, in infected cells. J. Virol. **82:**4471–4479.
50. **Neuman, B. W., D. A. Stein, A. D. Kroeker, M. J. Churchill, A. M. Kim, P. Kuhn, P. Dawson, H. M. Moulton, R. K. Bestwick, P. L. Iversen, and M. J. Buchmeier.** 2005. Inhibition, escape, and attenuated growth of severe acute respiratory syndrome coronavirus treated with antisense morpholino oligomers. J. Virol. **79:**9665–9676.
51. **Ng, M. L., S. H. Tan, E. E. See, E. E. Ooi, and A. E. Ling.** 2003. Early events of SARS coronavirus infection in vero cells. J. Med. Virol. **71:**323–331.
52. **Panesar, N. S.** 2003. Lymphopenia in SARS. Lancet **361:**1985.
53. **Peiris, J. S., S. T. Lai, L. L. Poon, Y. Guan, L. Y. Yam, W. Lim, J. Nicholls, W. K. Yee, W. W. Yan, M. T. Cheung, V. C. Cheng, K. H. Chan, D. N. Tsang, R. W. Yung, T. K. Ng, and K. Y. Yuen.** 2003. Coronavirus as a possible cause of severe acute respiratory syndrome. Lancet **361:**1319–1325.
54. **Raaben, M., M. J. Groot Koerkamp, P. J. Rottier, and C. A. de Haan.** 2007. Mouse hepatitis coronavirus replication induces host translational shutoff and mRNA decay, with concomitant formation of stress granules and processing bodies. Cell. Microbiol. **9:**2218–2229.
55. **Ren, L., R. Yang, L. Guo, J. Qu, J. Wang, and T. Hung.** 2005. Apoptosis induced by the SARS-associated coronavirus in Vero cells is replication-dependent and involves caspase. DNA Cell Biol. **24:**496–502.
56. **Reynolds, A., E. M. Anderson, A. Vermeulen, Y. Fedorov, K. Robinson, D. Leake, J. Karpilow, W. S. Marshall, and A. Khvorova.** 2006. Induction of the interferon response by siRNA is cell type- and duplex length-dependent. RNA **12:**988–993.
57. **Rhoads, R. E.** 1993. Regulation of eukaryotic protein synthesis by initiation factors. J. Biol. Chem. **268:**3017–3020.
58. **Ron, D., and P. Walter.** 2007. Signal integration in the endoplasmic reticulum unfolded protein response. Nat. Rev. Mol. Cell Biol. **8:**519–529.
59. **Savinova, O., and R. Jagus.** 1997. Use of vertical slab isoelectric focusing and immunoblotting to evaluate steady-state phosphorylation of eIF2 alpha in cultured cells. Methods **11:**419–425.
60. **Schaecher, S. R., E. Touchette, J. Schriewer, R. M. Buller, and A. Pekosz.** 2007. Severe acute respiratory syndrome coronavirus gene 7 products contribute to virus-induced apoptosis. J. Virol. **81:**11054–11068.
61. **Scheuner, D., R. Patel, F. Wang, K. Lee, K. Kumar, J. Wu, A. Nilsson, M. Karin, and R. J. Kaufman.** 2006. Double-stranded RNA-dependent protein kinase phosphorylation of the alpha-subunit of eukaryotic translation initiation factor 2 mediates apoptosis. J. Biol. Chem. **281:**21458–21468.
62. **Spiegel, M., A. Pichlmair, E. Muhlberger, O. Haller, and F. Weber.** 2004. The antiviral effect of interferon-beta against SARS-coronavirus is not mediated by MxA protein. J. Clin. Virol. **30:**211–213.
63. **Srivastava, S. P., K. U. Kumar, and R. J. Kaufman.** 1998. Phosphorylation of eukaryotic translation initiation factor 2 mediates apoptosis in response to activation of the double-stranded RNA-dependent protein kinase. J. Biol. Chem. **273:**2416–2423.
64. **Stein, D. A.** 2008. Inhibition of RNA virus infections with peptide-conjugated morpholino oligomers. Curr. Pharm. Des. **14:**2619–2634.
65. **Stertz, S., M. Reichelt, M. Spiegel, T. Kuri, L. Martinez-Sobrido, A. Garcia-Sastre, F. Weber, and G. Kochs.** 2007. The intracellular sites of early replication and budding of SARS-coronavirus. Virology **361:**304–315.
66. **Stojdl, D. F., N. Abraham, S. Knowles, R. Marius, A. Brasey, B. D. Lichty, E. G. Brown, N. Sonenberg, and J. C. Bell.** 2000. The murine double-stranded RNA-dependent protein kinase PKR is required for resistance to vesicular stomatitis virus. J. Virol. **74:**9580–9585.

67. **Summerton, J.** 1999. Morpholino antisense oligomers: the case for an RNase H-independent structural type. Biochim. Biophys. Acta **1489:**141–158.
68. **Summerton, J., and D. Weller.** 1997. Morpholino antisense oligomers: design, preparation, and properties. Antisense Nucleic Acid Drug Dev. **7:**187–195.
69. **Tahara, S. M., T. A. Dietlin, C. C. Bergmann, G. W. Nelson, S. Kyuwa, R. P. Anthony, and S. A. Stohlman.** 1994. Coronavirus translational regulation: leader affects mRNA efficiency. Virology **202:**621–630.
70. **Tan, Y. J., B. C. Fielding, P. Y. Goh, S. Shen, T. H. Tan, S. G. Lim, and W. Hong.** 2004. Overexpression of 7a, a protein specifically encoded by the severe acute respiratory syndrome coronavirus, induces apoptosis via a caspase-dependent pathway. J. Virol. **78:**14043–14047.
71. **Tan, Y. J., S. G. Lim, and W. Hong.** 2007. Regulation of cell death during infection by the severe acute respiratory syndrome coronavirus and other coronaviruses. Cell. Microbiol. **9:**2552–2561.
72. **Tan, Y. X., T. H. Tan, M. J. Lee, P. Y. Tham, V. Gunalan, J. Druce, C. Birch, M. Catton, N. Y. Fu, V. C. Yu, and Y. J. Tan.** 2007. Induction of apoptosis by the severe acute respiratory syndrome coronavirus 7a protein is dependent on its interaction with the Bcl-XL protein. J. Virol. **81:**6346–6355.
73. **Taylor, S. S., N. M. Haste, and G. Ghosh.** 2005. PKR and eIF2alpha: integration of kinase dimerization, activation, and substrate docking. Cell **122:**823–825.
74. **Versteeg, G. A., P. S. van de Nes, P. J. Bredenbeek, and W. J. Spaan.** 2007. The coronavirus spike protein induces endoplasmic reticulum stress and upregulation of intracellular chemokine mRNA concentrations. J. Virol. **81:**10981–10990.
75. **Wathelet, M. G., M. Orr, M. B. Frieman, and R. S. Baric.** 2007. Severe acute respiratory syndrome coronavirus evades antiviral signaling: role of nsp1 and rational design of an attenuated strain. J. Virol. **81:**11620–11633.
76. **Weber, F., V. Wagner, S. B. Rasmussen, R. Hartmann, and S. R. Paludan.** 2006. Double-stranded RNA is produced by positive-strand RNA viruses and DNA viruses but not in detectable amounts by negative-strand RNA viruses. J. Virol. **80:**5059–5064.
77. **Wei, L., S. Sun, C. H. Xu, J. Zhang, Y. Xu, H. Zhu, S. C. Peh, C. Korteweg, M. A. McNutt, and J. Gu.** 2007. Pathology of the thyroid in severe acute respiratory syndrome. Hum. Pathol. **38:**95–102.
78. **Wek, R. C., H. Y. Jiang, and T. G. Anthony.** 2006. Coping with stress: eIF2 kinases and translational control. Biochem. Soc. Trans. **34:**7–11.
79. **World Health Organization.** 2004, posting date. Summary of probable SARS cases with onset of illness from 1 November 2002 to 31 July 2003. http://www.who.int/csr/sars/country/table2004_04_21/en/index.html.
80. **Yan, H., G. Xiao, J. Zhang, Y. Hu, F. Yuan, D. K. Cole, C. Zheng, and G. F. Gao.** 2004. SARS coronavirus induces apoptosis in Vero E6 cells. J. Med. Virol. **73:**323–331.
81. **Yang, M., M. H. Ng, and C. K. Li.** 2005. Thrombocytopenia in patients with severe acute respiratory syndrome. Hematology **10:**101–105.
82. **Youngblood, D. S., S. A. Hatlevig, J. N. Hassinger, P. L. Iversen, and H. M. Moulton.** 2007. Stability of cell-penetrating peptide-morpholino oligomer conjugates in human serum and in cells. Bioconjug. Chem. **18:**50–60.
83. **Yuan, X., Y. Shan, Z. Zhao, J. Chen, and Y. Cong.** 2005. G0/G1 arrest and apoptosis induced by SARS-CoV 3b protein in transfected cells. Virol. J. **2:**66.
84. **Zhang, P., B. L. Jacobs, and C. E. Samuel.** 2008. Loss of protein kinase PKR expression in human HeLa cells complements the vaccinia virus E3L deletion mutant phenotype by restoration of viral protein synthesis. J. Virol. **82:**840–848.
85. **Zhang, P., and C. E. Samuel.** 2008. Induction of protein kinase PKR-dependent activation of interferon regulatory factor 3 by vaccinia virus occurs through adapter IPS-1 signaling. J. Biol. Chem.
86. **Zhang, P., and C. E. Samuel.** 2007. Protein kinase PKR plays a stimulus- and virus-dependent role in apoptotic death and virus multiplication in human cells. J. Virol. **81:**8192–8200.
87. **Zhang, Q. L., Y. Q. Ding, L. He, W. Wang, J. H. Zhang, H. J. Wang, J. J. Cai, J. Geng, Y. D. Lu, and Y. L. Luo.** 2003. Detection of cell apoptosis in the pathological tissues of patients with SARS and its significance. Di Yi Jun Yi Da Xue Xue Bao **23:**770–773.